Detecting the Higgs bosons of the minimal supersymmetric model

John F. Gunion and Lynne H. Orr
Department of Physics, University of California, Davis, California 95616
(Received 9 December 1991)

Detection of the neutral Higgs bosons of the minimal supersymmetric model (MSSM) in the $W+$ Higgs boson $+X\to l\gamma\gamma X$ final state is studied in detail and compared to the inclusive $\gamma\gamma$ discovery mode. The regions of model parameter space in which viable signals emerge at the Superconducting Super Collider (SSC) and CERN Large Hadron Collider (LHC) are determined and compared to the regions where the "gold-plated" $l^+l^-l^+l^-$ discovery mode can be utilized. The regions of parameter space where the detection of the charged Higgs boson in $t\to H^+b$ decays is likely to be possible are determined. Radiative corrections to the Higgs-boson masses and neutral sector mixing angle are included in our assessments. We come close to establishing a no-lose theorem: namely, throughout nearly all of parameter space one or more of the MSSM Higgs bosons can be discovered either at the CERN e^+e^- collider LEP II or using the above modes at the SSC or LHC, independent of the value of m_t. A brief survey of other interesting modes is also given.

PACS number(s): 13.85.Qk, 12.15.Cc, 14.80.Gt

I. INTRODUCTION

A. Intermediate-mass standard model (SM) Higgs boson—review

Future hadron supercolliders such as the Superconducting Super Collider (SSC) and CERN Large Hadron Collider (LHC) have been shown to provide a fairly ideal laboratory for the search for the standard model Higgs boson. (For reviews and references to older results see Ref. [1]; newer developments are surveyed in the reports of Refs. [2,3].) The mass region $2m_Z \lesssim m_{\phi^0} \lesssim 700-800$ GeV is easily probed via the "gold-plated mode $\phi^0\to ZZ\to l^+l^-l^+l^-$ ($4l$, for short). The $\phi^0\to ZZ^*\to 4l$ mode, first considered in Ref. [4], allows ϕ^0 detection for ~ 135 GeV $\lesssim m_{\phi^0} \lesssim 2m_Z$. However, until recently, a clear signal had proved elusive for Higgs-boson masses below ~ 135 GeV. For instance, inclusive ϕ^0 production, followed by $\phi^0\to\gamma\gamma$, leads to a viable signal in this region only if very excellent $\gamma\gamma$ mass resolution and γ-jet rejection is possible [4]. (For a recent experimentally oriented summary see Ref. [2].) A typical SSC detector, such as that proposed by the Solenoidal Detector Collaboration (SDC) [5], will not have the required resolution and jet rejection. The recent developments that have filled the $80 \lesssim m_{\phi^0} \lesssim 135$ GeV gap (the "intermediate mass" region) between the lower limit of the $ZZ^*\to 4l$ channel and the approximate upper limit for ϕ^0 discovery at the CERN e^+e^- collider LEP II focus on $W\phi^0$ associated production.

First, $W^*\to W\phi^0$ production followed by $W\to l\nu$ and $\phi^0\to\gamma\gamma$ was proposed as a relatively background-free channel [6,7,2]. Indeed, one finds that the backgrounds, primarily from $W\gamma\gamma$ and $W\gamma j$ continuum production [6,7], are substantially smaller than the signal. However, the event rate for $W^*\to W\phi^0\to l\gamma\gamma X$ is so low that an integrated luminosity of $L=100$ fb^{-1} (i.e., ten times the canonical SSC yearly luminosity) would have been required to achieve a significant signal for a ϕ^0 with mass between ~ 80 and ~ 150 GeV.

A dramatic improvement of the situation has been the observation [8,9] that this same $W\phi^0\to l\gamma\gamma X$ final state emerges from $t\bar{t}\phi^0$ production (which has a very substantial rate for moderate m_{ϕ^0}) in which one of the t's decays to the leptonically decaying W. The $l\gamma\gamma X$ rate due to the $t\bar{t}\phi^0$ process is about 4 to 5 times greater than that for the W^* process at the SSC. Further, the $t\bar{t}\gamma\gamma$ background has been shown to be small unless $m_t \lesssim 120$ GeV [10,11]. Still awaiting a fully quantitative study are the $t\bar{t}j$ and $t\bar{t}\gamma$ event rates. Below we shall compute a major component of the $t\bar{t}j$ background and crudely estimate the $t\bar{t}\gamma$ background. Our results suggest that these backgrounds should be manageable for a reasonable γ-jet rejection factor. Including the $W\gamma\gamma$, $t\bar{t}\gamma\gamma$, and $W\gamma j$ backgrounds (with a γ-j rejection factor of $R_{\gamma j}=5\times10^{-4}$), one obtains a viable ϕ^0 signal at the SSC throughout the $80 \lesssim m_{\phi^0} \lesssim 135$ GeV mass region for the canonical $L=10$ fb^{-1} of integrated luminosity. (At the LHC, L substantially above 10 fb^{-1} continues to be required, but the full 100 fb^{-1} enhanced luminosity is not necessary.) In fact, for $L=100$ fb^{-1} at the SSC, the event numbers are sufficient that the W^* and $t\bar{t}\phi^0$ processes can be separated from one another (by jet antitagging or tagging), thereby allowing separate determination of the $WW\phi^0$ and $t\bar{t}\phi^0$ couplings, respectively. (However, this is not possible at the LHC.) As a result, we can now say with confidence that the full intermediate mass range of the SM Higgs boson can be explored at the SSC.

B. Minimal supersymmetric standard model (MSSM) Higgs-boson sector

However, various theoretical arguments suggest that the sector responsible for electroweak symmetry breaking will be more complicated than the single doublet of the SM. Among the theoretical approaches which go beyond the standard model, the supersymmetric extension of the minimal standard model is particularly attractive in that

it preserves the elementarity of the Higgs bosons while at the same time solving the naturalness and hierarchy problems. In the *minimal* supersymmetric model (MSSM), the Higgs-boson sector consists of a two-doublet extension of the standard model. The MSSM Higgs-boson sector is automatically *CP* conserving, and the neutral Higgs scalars can be characterized as either *CP* even or *CP* odd. The *CP*-even neutral Higgs bosons are denoted by h^0 and H^0 (with $m_{h^0} \leq m_{H^0}$), and the *CP*-odd Higgs boson by A^0. In the context of the MSSM, current experimental data from LEP indicate that $m_{h^0} \gtrsim 40$ GeV, $m_{A^0} \gtrsim 30$ GeV. As we shall see below, these lower bounds will be pushed to near m_Z after LEP II completes its experimental search for $e^+e^- \to Z^* \to h^0 A^0$ or Zh^0.

The Higgs-boson sector of the MSSM is completely determined at tree level by specifying just two parameters, conventionally chosen to be m_{A^0} and $\tan\beta = v_2/v_1$. All other Higgs-boson masses as well as the neutral sector mixing angle α and all couplings to quarks and vector bosons can be expressed in terms of these parameters. In particular, one finds [1] that $m_{h^0} \leq m_Z$, and that production rates are such that LEP II would either discover the h^0 or rule out the MSSM [12,13]. However, at one loop [14–19], additional parameters are required to fully determine the masses and couplings of all the Higgs bosons. Aside from m_{A^0} and $\tan\beta$, values for m_t and a number of supersymmetric model parameters (squark masses, μ, and the $A_{b,t}$) must be specified. The most crucial result is that the one-loop corrections can boost m_{h^0} above m_Z, i.e., beyond the reach of LEP II, if $m_t \gtrsim 120$ GeV and $\tan\beta$ is not too small. If this occurs, then the h^0 must be searched for at the LHC and SSC using the techniques developed for an intermediate mass SM Higgs boson. More generally, it is important to determine the region of MSSM parameter space for which the LHC and SSC can find at least one of the MSSM Higgs bosons. Some examination of the relevant issues has already been given at tree level in Refs. [1–3] (see also references therein) and related experimental studies for the SSC, and in Ref. [20] and related experimental studies for the LHC. Other work, complementary to the present effort, has appeared in Ref. [21] and also is in progress [22].

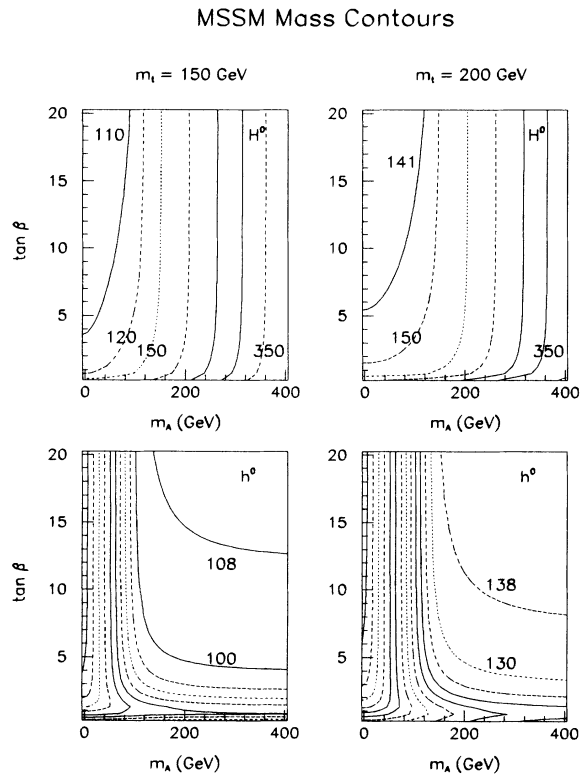

FIG. 1. Mass contours in the m_{A^0}-$\tan\beta$ parameter space for H^0 and h^0 with $m_t = 150$ and 200 GeV. The H^0 contours begin with 141 GeV (110 and 120 GeV) for $m_t = 200$ GeV (150 GeV), with the remaining contours being those for $m_{H^0} = 150$, 200, 250, 300, and 350 GeV. The h^0 contours run from 10 GeV in steps of 10 GeV to a maximum value of 130 GeV (100 GeV) for $m_t = 200$ GeV (150 GeV). These curves include the one-loop leading log radiative corrections with $m_{\tilde{q}} = 1$ TeV (squark mixing has been neglected).

Before proceeding, it is useful to further quantify the above remarks by repeating two of the graphs appearing in Ref. [21]. The impact of radiative corrections upon the masses of the MSSM Higgs bosons is illustrated by the mass contour plots of Fig. 1. There, we give mass contours for h^0 and H^0 in the m_{A^0}-$\tan\beta$ parameter space for $m_t = 150$ and 200 GeV (with $m_{\tilde{q}} = 1$ TeV and squark mixing neglected). Although LEP provides the lower bound for m_{A^0} noted earlier, there are currently no experimental constraints on $\tan\beta$. On the basis of renormalization group arguments it is generally expected that $1 \lesssim \tan\beta \lesssim m_t/m_b$ [1]. Thus, in this and future plots we have considered the range $0.5 \leq \tan\beta \leq 20$. Predictions (including radiative corrections) for the extent to which LEP II can probe the MSSM Higgs sector appear in Fig. 2. There, we plot event number contours for h^0Z and h^0A^0 associated production for $\sqrt{s} = 200$ GeV and an integrated luminosity of $L = 500$ pb^{-1}.[1] (A 25% detection efficiency is also included.) If one assumes that 25 observed events are needed for discovery, then there are substantial portions of parameter space for which discovery of the h^0 is not possible using either h^0Z or h^0A^0 associated production. For large m_t the region for which LEP II will discover the h^0 is quite restricted because the h^0 is simply too heavy.

C. MSSM Higgs-boson search strategies

In this paper we shall explore methods for detecting MSSM Higgs bosons, especially in the intermediate mass

[1]The results of Fig. 2 have been obtained using the complete leading log radiative corrections to the MSSM Higgs-boson masses and couplings given in Ref. [19]. It is interesting to note that the parameter space regions outlined in Fig. 2 are quite sensitive to the precise form of these corrections. For example, if one only includes the leading m_t^4 corrections, the region of parameter space where h^0 detection at LEP II is possible would shrink.

region. One major focus will be on the role of the W+Higgs boson+$X \to l\gamma\gamma X$ production/detection channel, which has been shown to be so useful for the SM ϕ^0. The MSSM case is more difficult, however, because the couplings of the h^0 and H^0 to $t\bar{t}$ and WW are in general suppressed compared to the corresponding SM couplings, as are the $\gamma\gamma$ branching ratios. The A^0 couplings and $\gamma\gamma$ branching ratio are suppressed except for $\tan\beta < 1$. Thus it is necessary to examine the MSSM case in detail to determine where in parameter space an observable $l\gamma\gamma$ signal is possible.

We shall show that a search in the $l\gamma\gamma X$ mode reduces considerably the region of parameter space for which there is a possibility of finding *no* MSSM Higgs bosons either at LEP II or at the SSC. The largest region for which the $l\gamma\gamma$ mode is required as a supplement to LEP II and the $4l$ mode at the SSC is that where m_{A^0} is large. For large m_{A^0} one finds that $m_{H^0} \simeq m_{H^+} \simeq m_{A^0}$, so that all three of these MSSM Higgs bosons could lie beyond the reach even of the SSC. If, in addition, m_t is large, then we see from Figs. 1 and 2 that the h^0 is quite likely

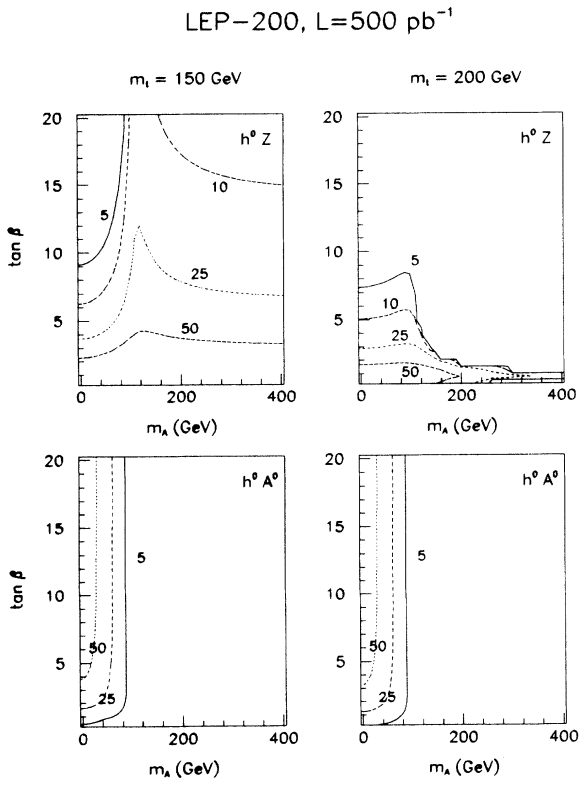

FIG. 2. Event number contours in m_{A^0}-$\tan\beta$ parameter space for $e^+e^- \to h^0 Z$ and $e^+e^- \to h^0 A^0$ at LEP II with $\sqrt{s} = 200$ GeV and an integrated luminosity of $L = 500$ fb^{-1}. Results are presented for the two top quark mass values of $m_t = 150$ and 200 GeV. We have taken $m_{\tilde{q}} = 1$ TeV and have neglected squark mixing. We have included an average detection efficiency factor of 25%. The event number for each contour shown is given on the figure. Assuming that discovery is possible if at least 25 events remain after including the detection efficiency, then there is a substantial region where neither process is viable.

(especially for large $\tan\beta$) to be sufficiently heavy that it could not be found at LEP or LEP II, despite the fact that it would have SM-like couplings in this limit. Furthermore, if m_t is not larger than about 170 GeV and $\tan\beta$ is moderate in size, one finds $m_{h^0} \lesssim 130$ GeV, i.e., below the region accessible via the $h^0 \to ZZ^* \to 4l$ final state. Thus, in this case h^0 detection at the SSC in any mode other than the $l\gamma\gamma X$ final state would be very difficult.

More generally, whenever $120 \lesssim m_t \lesssim 170$ GeV, $m_{A^0} \gtrsim m_Z$, and $\tan\beta \gtrsim 5$ (depending upon the precise value of m_t, squark masses, and other MSSM parameters) m_{h^0} could be above 100 GeV, and thus outside the reach of LEP II, but below the $\sim$ 130 GeV lower limit of the $4l$ mode. Detection of the H^0 and especially the A^0 in the $ZZ \to 4l$ final-state mode will also be problematical: for these parameter choices, the H^0 has suppressed couplings to vector boson pairs, and, of course, the CP-odd A^0 has no *tree-level* couplings to vector boson pairs—its VV couplings arise first at one loop. The exact regions of m_{A^0}-$\tan\beta$ parameter space in which one or both of the neutral CP-even MSSM Higgs bosons can be detected in the $4l$ mode have been delineated in Ref. [21]. (For earlier tree-level results, see Refs. [3,20].) The corresponding study for the A^0 appears in Ref. [23]. These results will be reviewed in more detail in Secs. III and V.

We shall find that the $l\gamma\gamma X$ mode provides an important complement to other detection modes for the MSSM Higgs bosons. At the SSC, we will see that it allows detection of the h^0 whenever $m_{A^0} \gtrsim 200$ GeV, more or less independent of m_t (for $m_t \geq 100$ GeV). As we shall discuss in detail in our conclusions, this implies that we will be able to see at least one, and often several, of the MSSM Higgs bosons at either LEP II or the SSC throughout almost all of m_{A^0}-$\tan\beta$ parameter space. In particular, the $l\gamma\gamma X$ discovery mode for the h^0 is of crucial importance for $120 \lesssim m_t \lesssim 170$ GeV, for which LEP II coverage is not complete and $h^0, H^0, A^0 \to 4l$ decays cannot be detected at the SSC in the bulk of the m_A^0-$\tan\beta$ parameter space.

Although the study of the $l\gamma\gamma$ mode comprises the largest component of the present work, we also consider the inclusive $\gamma\gamma$ detection mode [24]. We demonstrate that the $l\gamma\gamma$ mode should prove superior, given the expected integrated luminosities at the SSC and LHC, for even relatively optimistic $M_{\gamma\gamma}$ resolutions and jet-photon rejection factors, and certainly for the resolution and rejection factor that are believed to be representative of the SDC detector [5]. On another front, we will compare the region of parameter space for which the $l\gamma\gamma$ mode can be used to find one or more of the neutral MSSM Higgs bosons to that which can be explored using the $4l$ "gold-plated" final state as determined in Ref. [21]. Of course, detection of the charged Higgs boson would clearly establish the existence of a nonminimal Higgs sector. Thus we also determine the region of parameter space over which the branching ratio for $t \to H^+ b$ decay is sufficient that the H^+ of the MSSM could be detected in $t\bar{t}$ production events. A survey of the combination of the $l\gamma\gamma$, $4l$ and

$t \to H^+ b$ detection channels allows us to come close to demonstrating a no-lose theorem: one or more of the MSSM Higgs bosons can be detected either at LEP II or in one of the above three modes at the SSC, regardless of the value of m_t.

The organization of the paper is as follows. Section II presents various details of our $l\gamma\gamma$ computations, including the $\gamma\gamma$ branching ratios for the h^0, H^0, and A^0. In Sec. III we present the $l\gamma\gamma$ event rates and backgrounds and delineate the regions of m_{A^0}-tanβ parameter space for which h^0, H^0, or A^0 detection in the $l\gamma\gamma$ mode is possible. Three values of the top-quark mass will be analyzed in detail: $m_t = 100$, 150, and 200 GeV. Results for both the SSC and LHC will be presented. In Sec. IV, we present results for the inclusive $\gamma\gamma$ detection mode, including backgrounds. Comparisons to the $l\gamma\gamma$ mode are made. In Sec. V we analyze the complementarity between the $l\gamma\gamma$ mode and other techniques for detecting the various MSSM Higgs bosons. In particular, we compare the $l\gamma\gamma$ mode to the $4l$ mode for the neutral Higgs bosons, and show that detection of the charged Higgs boson in $t \to H^+ b$ decays should provide an important complement to these neutral-Higgs-boson discovery modes. Finally, in Sec. VI we give a brief overall conclusion and restate, with the necessary minor qualifications, the no-lose theorem.

II. COMPUTATIONAL DETAILS

A. MSSM Higgs-boson $\gamma\gamma$ branching ratios

A crucial ingredient in the rates for the $l\gamma\gamma X$ (and $\gamma\gamma X$) final state for each of the neutral MSSM Higgs bosons is their $\gamma\gamma$ branching ratio. Here we shall review the results obtained in Refs. [21,23]. The results to be presented can be compared to the $\gamma\gamma$ branching ratio for the SM ϕ^0 which, in the intermediate mass range, varies between a few $\times 10^{-4}$ to 2×10^{-3}. As for the figures presented in Sec. I, we shall employ the one loop radiative corrections to Higgs-boson masses and couplings given in the leading log approximation in Ref. [19], assuming a squark mass of 1 TeV and neglecting squark mixing. In Figs. 3–5 we show $B(h^0, H^0, A^0 \to \gamma\gamma)$ as a function of Higgs-boson mass at fixed values of tanβ=0.5, 1, 2, 3.5, and 5. Here and below we present results for $m_t = 100$, 150, and 200 GeV. Results for $m_t = 150$ GeV may be considered "representative," as this m_t is near the value expected from precision electroweak measurements, and results for $m_t = 100$ and 200 GeV illustrate the variation with top-quark mass. Included in the computations are such subtleties as QCD corrections to the $b\bar{b}$ decay widths of the neutral Higgs boson, and inclusion of the most important one-loop decay channel, namely gg. Decays to pairs of supersymmetric particles are assumed to be kinematically forbidden, and charginos and squarks are assumed to be sufficiently heavy that their loops do not contribute to the

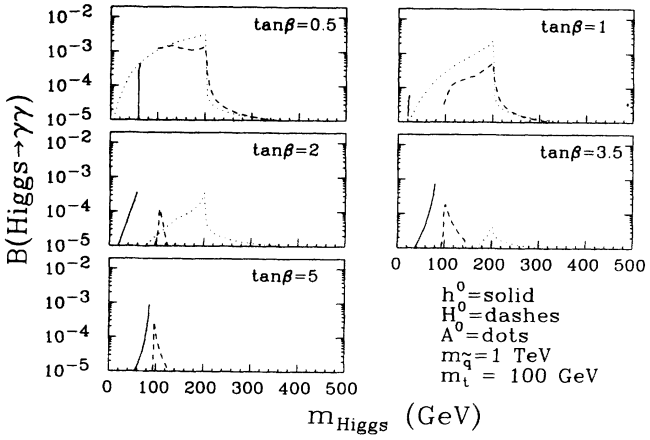

FIG. 3. $B(h^0, H^0, A^0 \to \gamma\gamma)$ as a function of Higgs-boson mass for $m_t = 100$ GeV and $m_b = 4.7$ GeV, for various tanβ values. QCD corrections to the $b\bar{b}$ width are included using Eqs. (2.7)–(2.9) of Ref. [1] with $\Lambda_{\overline{\rm MS}} = 0.19$ GeV, where $\overline{\rm MS}$ denotes the modified minimal subtraction scheme. Radiative corrections are included using the formulas of Ref. [19]. Supersymmetric parameters are chosen as specified in the text.

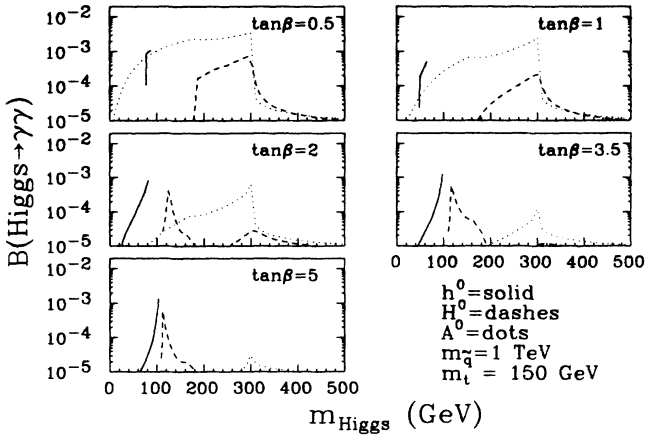

FIG. 4. Same as in Fig. 3, but for $m_t = 150$ GeV.

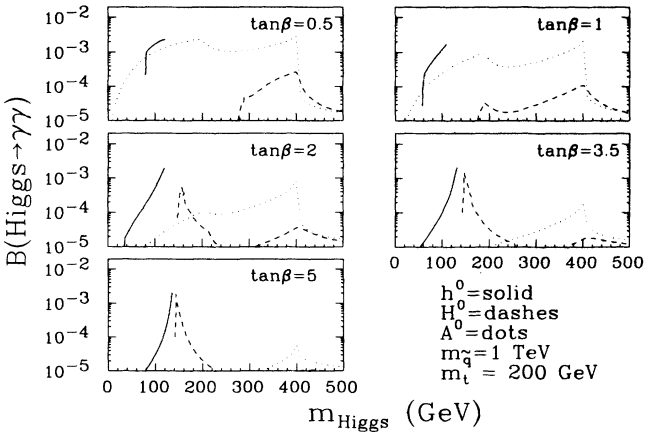

FIG. 5. Same as in Fig. 3, but for $m_t = 200$ GeV.

$\gamma\gamma$ couplings of the Higgs bosons.

Let us discuss briefly the major features of Figs. 3–5; see also Refs. [21,23]. First, consider Fig. 4 with $m_t = 150$ GeV.

(1) The narrow h^0 mass range is reflected in Fig. 4 in the limited extent of the h^0 curves (shown as solid lines). The steepness of the $\gamma\gamma$ branching ratio curves results from the fact that a large increase in m_{A^0} yields only a small increase in m_{h^0} but leads to a substantial increase in the $\gamma\gamma h^0$ coupling as the h^0 tree-level couplings approach their SM-like limits.

(2) The $\gamma\gamma$ branching ratios of the H^0 (dashed lines) and A^0 (dotted lines) fall off sharply above the $t\bar{t}$ threshold at 300 GeV.

(3) The H^0 branching ratios look qualitatively different for low versus high values of $\tan\beta$. For $\tan\beta = 0.5$, the $\gamma\gamma$ branching ratio is suppressed for $m_{H^0} \leq 180$ GeV because, below that mass, decays to ZA^0 and/or H^+H^- are allowed. (In general, the width for H^0 decay to any pair of Higgs bosons, H^+H^-, A^0A^0, or h^0h^0, is large when allowed by kinematics.) For higher $\tan\beta$, e.g., $\tan\beta = 2$, there is a peak at around 120 GeV corresponding to a narrow window in m_{H^0} in which decays to A^0A^0 are disallowed but decays to h^0h^0 are not yet possible.

(4) The $A^0 \to \gamma\gamma$ branching ratio decreases with increasing $\tan\beta$, both because of the increasing width for the $A^0 \to b\bar{b}$ channel and also because of the decreasing magnitude of the t-loop contribution to the $A^0\gamma\gamma$ coupling. (Recall that the $A^0 b\bar{b}$ coupling is proportional to $\tan\beta$ while the $A^0 t\bar{t}$ coupling is proportional to $\cot\beta$.)

The variation of the $\gamma\gamma$ branching ratios with m_t can be seen by comparing Figs. 3–5. Several important trends are evident. First, for larger m_t, m_{h^0} asymptotes to a higher value at large m_{A^0}, and so the branching ratio curves get shifted to higher m_{h^0} values. Also the asymptotic value of the $\gamma\gamma$ width of the h^0 ($\propto m_{h^0}^3$) is relatively larger than that for the $b\bar{b}$ channel ($\propto m_{h^0}$) at higher m_{h^0}, resulting in an increase in the $\gamma\gamma$ branching ratio. Second, as m_t increases, the $t\bar{t}$ threshold in H^0 and A^0 decays increases, expanding the region where $\gamma\gamma$ decays can be important. In addition, the maximum $\gamma\gamma$ branching ratio that can be achieved increases somewhat.

The ranges of Higgs mass for which $\gamma\gamma$ decays (and hence the $l\gamma\gamma X$ detection mode) might be useful can be inferred from the results of Figs. 3–5. Roughly, one requires that the $\gamma\gamma$ branching ratio be not too much below 10^{-3} (i.e., near the SM values) in order that the event rate at the SSC be adequate for detection in a few years of running time at the standard yearly integrated luminosity of $L = 10\ \text{fb}^{-1}$.

B. Signal and background cross-section calculations

We will now turn to a discussion of the other ingredients required for a quantitative determination of those regions of m_{A^0}-$\tan\beta$ parameter space for which detection of each of the neutral Higgs bosons is possible in the $l\gamma\gamma X$ mode.

In computing the $W^* \to W +$ Higgs boson and $gg \to t\bar{t} +$ Higgs boson production rates, we employ the Harriman-Martin-Roberts-Stirling set B parton distribution functions [25]. (The variation of event rate with the distributions chosen, illustrated for the ϕ^0 in Ref. [8], does not significantly affect our results.) The cuts employed are similar to those used in Ref. [8]:

$$p_T(l,\gamma) > 20\ \text{GeV}\ , \quad |\eta(l,\gamma)| < 2.5\ , \qquad \Delta R(\gamma_1,\gamma_2) > 0.4\ , \quad \Delta R(l,\gamma) > 0.4\ . \tag{1}$$

These cuts are designed to eliminate possible backgrounds, and are shown to do so quite successfully in Refs. [6,7,10,11], while retaining the bulk of the signal events for Higgs-boson masses below ~ 150 GeV. Since we shall also be interested in larger Higgs-boson masses, we have explored the extent to which the p_T cuts on the photons can be increased as the Higgs boson mass increases without any significant loss of signal event rate. We find, for instance, that at Higgs-boson masses of 250, 300, and 400 GeV we can require $p_T(\gamma) > 40$, 50, and 60 GeV without any significant loss of event rate beyond the rate obtained with the cuts of Eq. (1). The background rates quoted below will include this mass-dependent p_T cut on the photon. (Background results at Higgs-boson masses other than those quoted above are obtained by interpolation.) The event rates for signal and background will include a sum over final states with $l = e^+, e^-, \mu^+, \mu^-$. In the case of the $t\bar{t} +$ Higgs boson $\to W +$ Higgs boson X signal process and the $t\bar{t}\gamma\gamma$ background, the additional jets or charged lepton from the second W decay and the b jets are all required to be isolated from the tagged l, γ_1, and γ_2 by $\Delta R > 0.4$.

We note that for many parameter choices, $t \to H^+ b$ decays are kinematically allowed. In such cases, the reduced $t \to Wb$ branching ratio has been included in our computation of the signal event rates. We have erred on the conservative side by not including this reduction in the $t\bar{t}\gamma\gamma$ background rates. In any case, the $t \to H^+ b$ branching ratio is $\leq 20\%$ in all of the $\tan\beta > 1$ portion of the parameter space that we consider.

In determining the detectability of the Higgs-boson signal in the $l\gamma\gamma X$ channel, a critical ingredient is, of course, the resolution in the photon-photon invariant mass $M_{\gamma\gamma}$. In Ref. [7] it was found that a bin size of about 4 GeV was adequate to contain nearly all of the Higgs-boson signal events for Higgs-boson masses up to 130 GeV, assuming SDC detector resolutions. At a mass of 140 GeV a bin size of order 5 GeV is required. In order to extend these results to higher $M_{\gamma\gamma}$, we have explicitly computed the mass distribution using SDC detector resolutions, as specified in Ref. [5] and as employed in Ref. [7], at Higgs-boson masses of 200, 300, 400, and 500 GeV. The bin sizes required to contain essentially all of the Higgs-boson signal events at various masses are listed below (GeV units):

$M_{\gamma\gamma}$:	≤ 110,	140,	200,	300,	400,	500,
$\Delta M_{\gamma\gamma}$:	4,	5,	6,	10,	12,	14.

(2)

To a good approximation, these results correspond to a 3% bin size at high $M_{\gamma\gamma}$. These bin sizes were employed

in computing the background event levels. (Bin sizes appropriate for $M_{\gamma\gamma}$ values above 140 GeV other than those listed are computed by interpolation.)

The $M_{\gamma\gamma}$ distributions (after the cuts discussed above) for the $W\gamma\gamma$ and $W\gamma j$ backgrounds were provided by the author of Ref. [7], and those for the $t\bar{t}\gamma\gamma$ background were made available to us by the authors of Ref. [11]. After adjusting for the $M_{\gamma\gamma}$ bin sizes given above, and multiplying the $W\gamma j$ rate by a γ-jet rejection factor of $R_{\gamma j}=5\times10^{-4}$, we obtain the background event rates given in Fig. 6. The total background rate B for a given Higgs-boson mass and m_t is obtained by taking the sum of the $W\gamma\gamma+W\gamma j$ and $t\bar{t}\gamma\gamma$ event rates. Note that these are parton-level results and do not include detailed simulations of detector-dependent responses. An analysis of the SM Higgs-boson case (including backgrounds) specific to the SDC detector can be found in Ref. [26].

We have also considered the backgrounds from top events in which one or two jets are misidentified as a photon. In particular, we have calculated the "$M_{\gamma\gamma}$" distributions from $t\bar{t}g$ events in which both the gluon and one of the quarks from the nonleptonically decaying W appear to be photons. Using the cuts, resolution, and γ-jet rejection factor specified above, we find this background to be negligible. A potentially more serious background arises from $t\bar{t}\gamma$ events in which a single jet (either from the nonleptonically decaying W or from initial/final-state radiation) fakes a photon. We can obtain a rough estimate of this by rescaling the $t\bar{t}g$ event rate by coupling constant ratios. In that case it appears that for low m_t (~100 GeV) this background may contribute handfuls of events per SSC year. While not negligible, we estimate that this rate is smaller than the $t\bar{t}\gamma\gamma$ background (see Fig. 6). Furthermore, this background rate decreases with increasing top mass, and is smaller by about an order of magnitude for $m_t=200$ GeV than for $m_t=100$ GeV. Therefore, we expect the $t\bar{t}\gamma$ background to matter only for lower values of m_t, where, in any case, detection of the h^0 at LEP II should be possible. Since we have not performed a detailed calculation, the $t\bar{t}\gamma$ background is not included in the results we present.

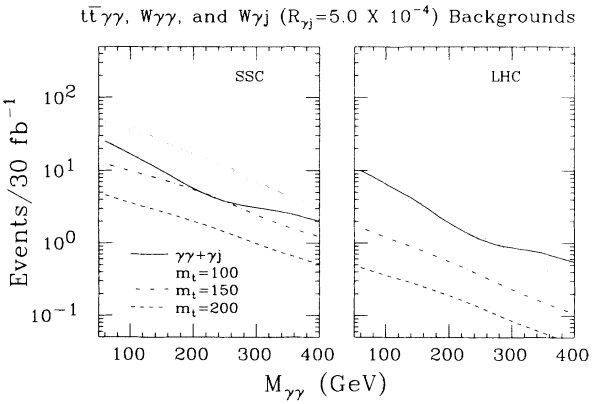

FIG. 6. The $W\gamma\gamma+W\gamma j$ and $t\bar{t}\gamma\gamma$ background event rates are plotted as a function of Higgs-boson mass for both the SSC and the LHC. In normalizing the $W\gamma j$ background we assumed $R_{\gamma j}=5\times10^{-4}$. In the case of the $t\bar{t}\gamma\gamma$ background results for $m_t=100$, 150, and 200 GeV are presented. The $M_{\gamma\gamma}$ bin size employed as a function of mass is specified in the text. All rates include the $W\to l\nu$ ($l=e\mu$) branching ratio. In the case of the $t\bar{t}\gamma\gamma$ background, either top was allowed to decay to the leptonically decaying W.

Before concluding this section, we wish to specify more precisely the criterion that we shall employ in assessing the observability of a $l\gamma\gamma X$ mode signal for one of the neutral MSSM Higgs bosons. Since we assume that in an experiment the above background event rates can be normalized away from the region of any possible Higgs-boson signal, the statistical significance of a given rate S for Higgs-boson production and decay into the $l\gamma\gamma$ final state is computed as $\sigma=S/\sqrt{B}$. We shall presume that any signal with $\sigma\geq4$ will be detectable. The implications of this criterion in terms of event rates may be read off of Fig. 6. At the SSC with $L=30$ fb^{-1}, for $m_t=100$, 150, and 200 GeV, $\sigma=4$ corresponds to $S\sim35,25,22$ at $M_{\gamma\gamma}\sim60$ GeV, $S\sim26,19,17$ at $M_{\gamma\gamma}\sim120$ GeV, and $S\sim10,8,7$ when $M_{\gamma\gamma}\sim350$ GeV. For $m_t\gtrsim150$ GeV and $\sigma=4$, S/B varies from about $\frac{2}{3}$ at low $M_{\gamma\gamma}$ to about 2 at high $M_{\gamma\gamma}$. Most of our $\sigma\geq4$ regions will correspond to Higgs-boson masses (i.e., $M_{\gamma\gamma}$ values) between about 60 and 120 GeV. There, we always have a substantial number of signal events and S/B between $\frac{1}{2}$ and 1. In the next section, we shall present contours of σ for $L=30$ fb^{-1}. The reader can reinterpret these contours to correspond to any desired choice of L. For instance, at $L=10$ fb^{-1} (a single year's canonical luminosity) a $\sigma=4$ signal corresponds to a $\sigma=7$ signal at $L=30$ fb^{-1}, i.e., a rescaling by the square root of L.

III. RESULTS FOR THE $l\gamma\gamma X$ MODE

Our results for the SSC are illustrated for the three m_t values of 100, 150, and 200 GeV in Figs. 7, 8, and 9. There we present the combined event rates from the $W^*\to W+$Higgs boson and $t\bar{t}+$Higgs boson processes for a net integrated luminosity of $L=30$ fb^{-1}, or three canonical SSC years. For comparison, rates for the intermediate mass SM ϕ^0 fall in the range of 40–80 events for this integrated luminosity. Also shown is the number of events required for a $\sigma=4$ statistical significance above background (dotted lines). The background has been computed as described in Sec. II B and the $\sigma=4$ event rates were already outlined there. The total widths of the H^0 and A^0 are considerably smaller than the bin sizes employed (see Sec. II) so long as $t\bar{t}$ decays are not allowed.[2]

Let us begin by discussing the h^0 results, shown as solid lines in Figs. 7–9. It is clear from Figs. 7–9 that as

[2]As the mass increases above the $t\bar{t}$ decay threshold, the widths of H^0 and A^0 grow quickly. However, in the region of parameter space considered here they are never larger than the bin sizes employed. In any case, the $\gamma\gamma$ branching ratios also decline very rapidly and the $l\gamma\gamma X$ detection mode is never viable much above $t\bar{t}$ threshold.

m_{h^0} asymptotes to its upper limit at a given tanβ (i.e., as m_{A^0} gets large), the $l\gamma\gamma X$ signal for the h^0 nearly always becomes observable. The only exception is for small tanβ at $m_t = 100$ GeV. In fact, the event rate slowly approaches the SM value found for $m_{\phi^0} = m_{h^0}$—even though m_{h^0} increases very little, its couplings are slowly approaching SM-like values. Increasing the top mass improves prospects for h^0 detection because the signal increases while the background decreases. We shall reinterpret these results in terms of the m_{A^0}-tanβ parameter space shortly.

Turning to the H^0 and A^0, we see from Figs. 7–9 that for tan$\beta \lesssim 1$ detection of the A^0 (solid lines) over a broad range of masses (below $2m_t$) is at least marginally possible. Indeed, for tan$\beta = 0.5$ we expect *more* events than for the SM ϕ^0. But by tan$\beta = 2$, detection of the A^0 in the $l\gamma\gamma$ final state becomes completely impossible. Detection of the H^0 (dashed lines) is generally only possible in two distinct regions: for large tanβ in the narrow range of m_{H^0} where the $H^0 \to \gamma\gamma$ branching ratio peaks, and for tan$\beta < 1$ when $m_{H^0} < 2m_t$. As implied above, increasing m_t extends the accessible region to higher Higgs-boson mass for both H^0 and A^0. For the H^0, the

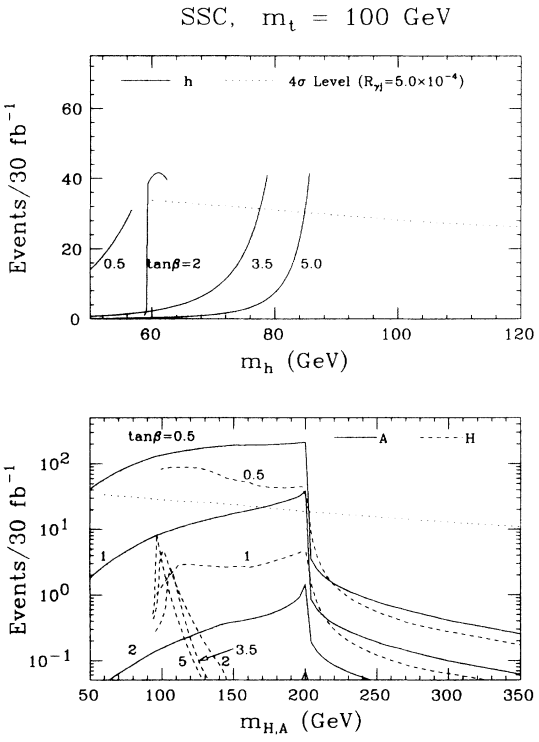

FIG. 7. $l\gamma\gamma X$ event rates as a function of Higgs-boson mass in comparison to the level required for a $\sigma = 4$ effect (shown as the dotted curves in the two plots). The values of tanβ corresponding to each curve are indicated: tanβ values of 0.5, 1, 2, 3.5, and 5 are considered. (If a curve does not appear for some tanβ value for a given Higgs boson, it is because it was outside the plot region.) Scans in m_{h^0} and m_{H^0} were performed by varying the A^0 mass in the range $0 \le m_{A^0} \le 400$ GeV. For this figure we take $m_t = 100$ GeV.

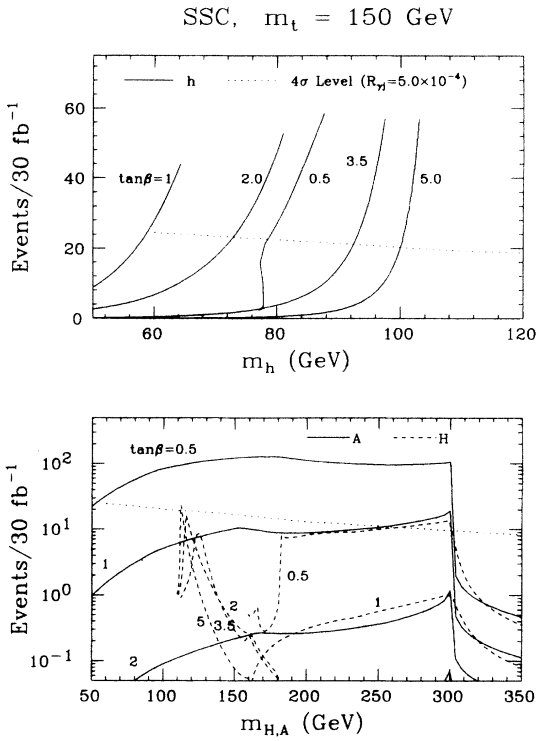

FIG. 8. Same as in Fig. 7, but for $m_t = 150$ GeV.

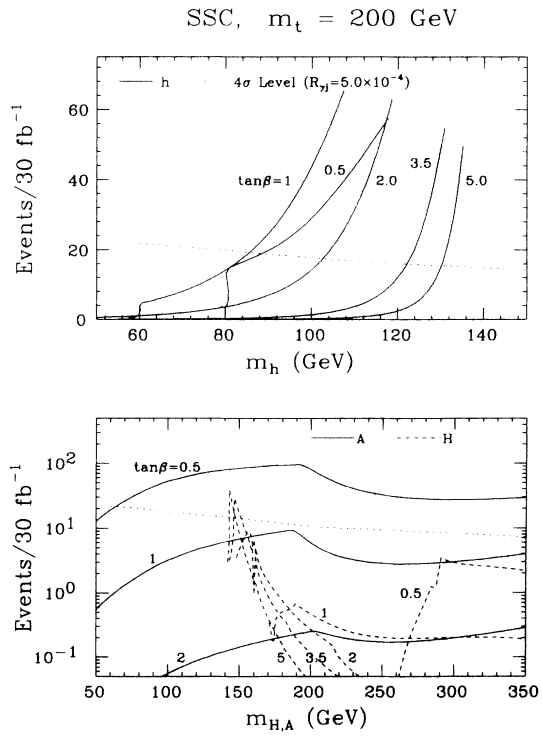

FIG. 9. Same as in Fig. 7, but for $m_t = 200$ GeV.

signal event rates increase with increasing m_t, while for the A^0 the rates decrease, constraining the accessible range of $\tan\beta$ to smaller values.

Turning briefly to the LHC, the corresponding plots to Figs. 7–9 are quite similar with the exception that both the signal event rates at $L=30$ fb^{-1} and the signal to background ratios are significantly smaller. In particular, the $t\bar{t}$ Higgs-boson associated production cross section falls very rapidly, namely by about a factor of about 6, in going from the SSC to the LHC. Since the W^* rate falls more slowly with decreasing energy, the W^* and $t\bar{t}$ Higgs-boson event rates become roughly comparable to each other at the LHC. To illustrate the SSC-LHC differences, we present in Fig. 10 the results for the LHC at $L=30$ fb^{-1} in the case of $m_t=150$ GeV; the backgrounds have been shown in Fig. 6.

In order to compare the potential of the $l\gamma\gamma X$ mode for the SSC and LHC, and to compare to LEP II and other SSC/LHC detection modes for the MSSM Higgs bosons, it is convenient to present our results for the $l\gamma\gamma X$ mode using contour plots in m_{A^0}-$\tan\beta$ parameter space. Contours of constant $\sigma=S/\sqrt{B}$ for both the SSC and LHC are presented in Figs. 11, 12, and 13 for $m_t=100$, 150, and 200 GeV, respectively. An integrated luminosity of $L=30$ fb^{-1} is employed for both machines. Let us reiterate some of our earlier conclusions for the SSC. First, it is apparent that $\sigma\geq 4$ for the h^0 for $m_{A^0}\gtrsim 200$ GeV so long as $m_t\gtrsim 150$ GeV. For m_t near 100 GeV, $m_{A^0}\gtrsim 250$ GeV and $\tan\beta\gtrsim 2$ is required for h^0 detection. H^0 detection in the $l\gamma\gamma X$ mode is confined to two narrow regions: one in the vicinity of $m_{A^0}=50-60$ GeV with $\tan\beta\gtrsim 1.5$ (a 4σ signal requires larger $\tan\beta$ and $m_t\geq 150$ GeV), and a second region where $m_{A^0}\lesssim 2m_t$ with $\tan\beta\lesssim 1$. A^0 detection in the $l\gamma\gamma X$ mode requires $m_{A^0}<2m_t$ (and $\gtrsim 60$ GeV) and $\tan\beta\lesssim 1-1.5$.

For the LHC, the $\sigma\geq 4$ regions shrink significantly, especially in the case of the h^0. For the h^0, $\sigma\geq 4$ is not achieved when $m_t=100$ GeV in any of the m_{A^0}-$\tan\beta$ parameter space region considered. For $m_t=150$ GeV the $\sigma\geq 4$ region is confined to $m_{A^0}\gtrsim 280$ GeV and $\tan\beta\gtrsim 2$. And for $m_t=200$ GeV the $t\bar{t}h^0$ production cross section at the LHC declines to a level such that $\sigma\geq 4$ is only achieved for a wedge of large m_{A^0} and small $\tan\beta$. Of course, if $L=60-100$ fb^{-1} can be achieved at the LHC (without increasing the background/signal ratio in the $l\gamma\gamma X$ mode), then regions in Figs. 11–13 with $\sigma\geq 3-2$ will allow detection. The contour plots make it clear that on the whole the LHC would then be roughly competitive with the SSC at $L=20-30$ fb^{-1}.

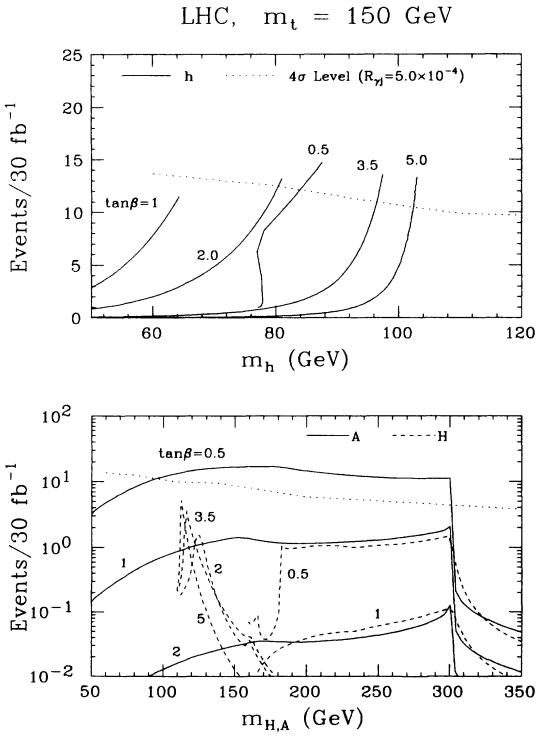

FIG. 10. Same as for Fig. 8, but for $\sqrt{s}=16$ TeV.

IV. THE INCLUSIVE $\gamma\gamma$ MODE

As discussed in the Introduction, it has already been demonstrated that detection of the SM ϕ^0 in the $\gamma\gamma$ decay mode of an inclusively produced ϕ^0 requires *extreme-*

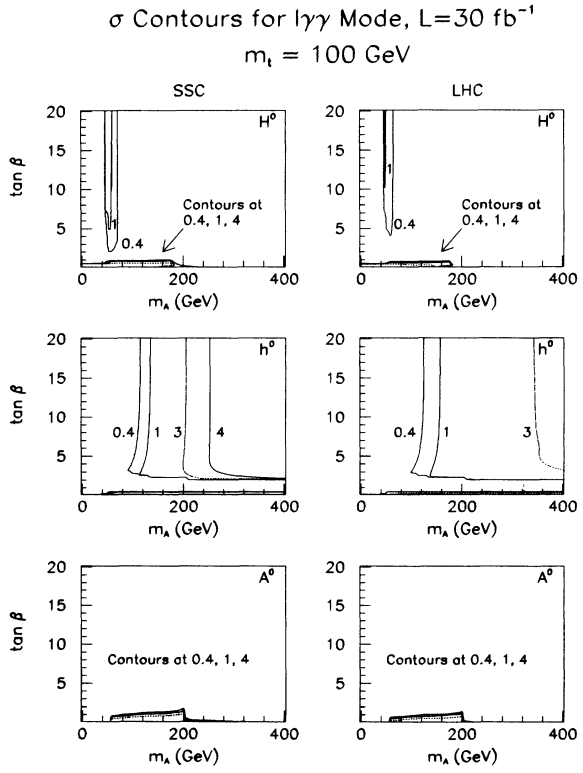

FIG. 11. Contour plots of $\sigma=S/\sqrt{B}$ for H^0, h^0, and A^0 detection in the $l\gamma\gamma X$ mode. Results are given for both the SSC and LHC assuming an integrated luminosity of $L=30$ fb^{-1}. We take $m_t=100$ GeV. Values of σ for each contour are indicated on the plots. For $\sigma\geq 4$ the $l\gamma\gamma X$ detection mode for the given Higgs boson should be viable.

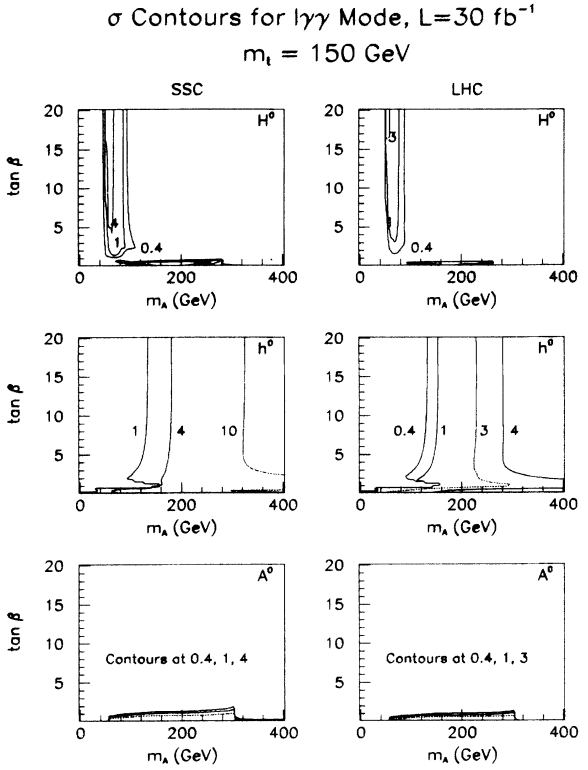

FIG. 12. Same as for Fig. 11, but for $m_t = 150$ GeV.

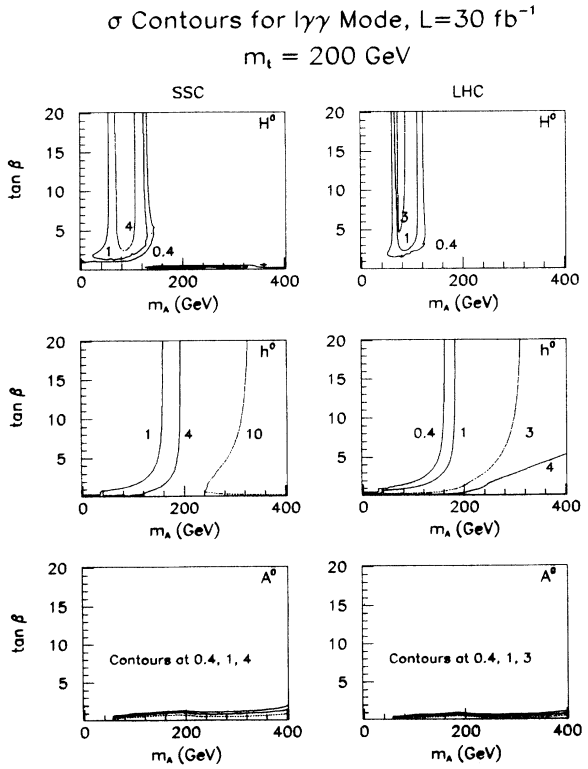

FIG. 13. Same as for Fig. 11, but for $m_t = 200$ GeV.

ly optimistic assumptions about $\gamma\gamma$ mass resolution and γ-jet rejection. In the MSSM (see Figs. 3–5), $\gamma\gamma$ branching ratios and couplings for the H^0 and A^0 can be larger than those for a ϕ^0 of the same mass in some regions of parameter space, and the $\gamma\gamma$ branching ratio of the h^0 can closely approach a SM-like value. Thus it is worthwhile to quantitatively examine the inclusive $\gamma\gamma$ detection mode for the h^0, H^0, and A^0. In particular, we are interested in comparing results for the inclusive mode to those for the $l\gamma\gamma$ mode discussed earlier, in order to determine whether the latter mode remains the more promising in the MSSM context.

A. Signal and background cross sections

Inclusive Higgs boson production is computed as in Ref. [21] as the sum of $gg \to$Higgs boson fusion (via quark loops), $gg \to b\bar{b}$ Higgs boson and $gg \to t\bar{t}$ Higgs boson. The latter process is, of course, the same as considered for the $l\gamma\gamma$ mode, except that in the inclusive rate we do not require that either of the t quarks be triggered upon in any way. The $gg \to t\bar{t}$ Higgs boson cross section is always substantially smaller than that deriving from direct one-loop fusion $gg \to$Higgs boson. In computing this latter process, squark loops with $m_{\tilde{q}} \sim 1$ TeV are not important—of course, a new heavy fermion family would greatly increase the rate. The $gg \to b\bar{b}$ Higgs boson cross section will be computed in the $b\bar{b} \to$Higgs boson fusion approximation appropriate when the Higgs-boson mass is substantially larger than m_b (as is always the case for mass regions of interest here–see Refs. [21,27] for more discussion). The $b\bar{b}$ fusion cross section is quite important at lower values of the Higgs-boson mass, and can even dominate gg fusion for large $\tan\beta$.

For the background, we shall consider only the $q\bar{q}, gg \to \gamma\gamma$ continuum. As often discussed (see, for example, Ref. [2]), this may in reality be a highly optimistic procedure since jet-jet and jet-photon backgrounds are very large and can only be suppressed below the $\gamma\gamma$ continuum if a jet-photon discrimination factor of order $R_{\gamma j} \sim 10^{-4}$ can be achieved. To achieve such a small $R_{\gamma j}$ requires the ability to distinguish a jet in which most of the energy is carried by a π^0 from a truly isolated photon. Whether the theoretical cuts proposed in the literature (see, e.g., Ref. [28]) can be as effective in a realistic detector as required is still a subject of debate.

As first noted in Ref. [4], the $\gamma\gamma$ continuum background can be greatly reduced by requiring that the photons emerge with a significant angle with respect to the beam (as measured in the $\gamma\gamma$ rest frame). We shall require $|\cos\theta^*| < 0.5$. For such a cut, nearly all of the photons will also fall into the $|y| < 3$ acceptance of a typical detector. (A less severe cut on $|\cos\theta^*|$ could be appropriate for a detector with larger acceptance.) We have included the $gg \to \gamma\gamma$ process [29] in only an approximate fashion by multiplying the $q\bar{q} \to \gamma\gamma$ continuum by a factor of 2. However, this is a fairly good (if sometimes slightly conservative) assumption for the $\cos\theta^*$ cut employed [29]. In computing the $\gamma\gamma$ continuum background event rate we employ the $\Delta M_{\gamma\gamma}$ resolutions specified earlier in Eq. (2). The resulting background

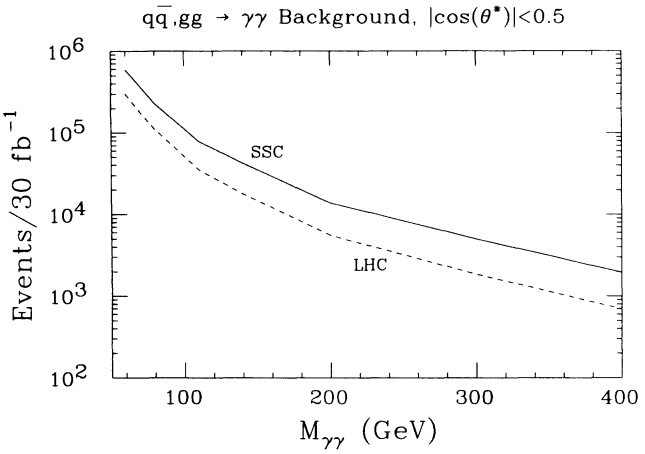

FIG. 14. The $\gamma\gamma$ background rate as a function of $M_{\gamma\gamma}$ computed as $L\{2[d\sigma(q\bar{q}\to\gamma\gamma)]/dM_{\gamma\gamma}\}\Delta M_{\gamma\gamma}$, with $\Delta M_{\gamma\gamma}$ from Eq. (2) and $L=30$ fb^{-1}. Results are given for both the SSC and LHC. $|\cos\theta^*|<0.5$ is required for the outgoing photons in the $\gamma\gamma$ rest frame.

event rates at the SSC and LHC as a function of $M_{\gamma\gamma}$ are presented for $L=30$ fb^{-1} in Fig. 14. The small variation with m_t arising from the $gg\to\gamma\gamma$ top-loop contribution is neglected.

B. Analysis and comparison to $l\gamma\gamma$

Assuming that the $\gamma\gamma$ continuum background can be well normalized away from any possible Higgs-boson signal, we use the same measure $\sigma=S/\sqrt{B}$ of signal significance as in the $l\gamma\gamma X$ analysis. The only cut applied to signal and background is that already discussed above, $|\cos\theta^*|<0.5$, and included in the rates of Fig. 14. For a real detector, there will undoubtedly be additional detector related efficiencies, not to mention those associated with achieving the $R_{\gamma j}\sim 10^{-4}$ jet-photon discrimination factor required. Thus our results for σ should be considered optimistic. Contour plots of σ in m_{A^0}-tanβ parameter space appear in Figs. 15 and 16. Results are given there for all three of the MSSM neutral Higgs boson H^0, h^0, and A^0, for both the SSC and LHC and for top-quark masses of $m_t=150$ and 200 GeV.

These results may now be compared to those for the $l\gamma\gamma$ mode given in Figs. 12 and 13 (keeping in mind that the $\gamma\gamma$ analysis is less thorough and more optimistic). We note that the $\sigma=4$ contours (which we felt represented a reasonable discovery criterion in the case of the $l\gamma\gamma$ mode) fall in similar locations. However, the inclusive $\gamma\gamma$ mode signal will in actuality be much harder to isolate. First, there is our neglect of efficiencies associated with additional cuts that will undoubtedly be needed to properly isolate the events of interest–i.e., the analogues of Eq. (1). Second, there is the neglect of γ-j and j-j backgrounds, which were included in our considerations for the $l\gamma\gamma$ mode for a fairly conservative choice ($R_{\gamma j}=5\times10^{-4}$) of the γ-j rejection factor. Third, but perhaps most importantly, there is the simple issue of whether a small bump in the $\gamma\gamma$ continuum can be seen for a σ of just 4. For example, at $M_{\gamma\gamma}=120$ GeV the $\gamma\gamma$ continuum event rate from Figs. 14 is 6.4×10^4. A $\sigma=4$ signal corresponds to an excess of about 1011 events in a mass bin of size 4 GeV. Such a 2% fluctuation is likely to prove rather difficult to find. Even $\sigma=8$ represents only a 3% fluctuation, and is seldom achieved in Figs. 15 and 16, even at the SSC. It is probably a better estimate of when a Higgs boson will lead to a clearly observable fluctuation in the presence of such a very large background rate.

This situation is to be contrasted with that for the $l\gamma\gamma$ mode. There, for $m_t\gtrsim 150$ GeV the $\sigma=4$ contours at the SSC correspond to S/B ranging from $\sim\frac{2}{3}$, with of order $S\sim25$ signal events, to ~2.5 with $S\sim6.5$ (at $L=30$ fb^{-1}—see Fig. 6 and the discussion at the end of Sec. II B). Although the number of signal events is smaller, the fact that the background level is intrinsically very low makes the $l\gamma\gamma$ signal more easily observable. Indeed, as noted earlier, most of the $\sigma\geq4$ regions in Figs. 11–13 for the $l\gamma\gamma$ mode correspond to Higgs-boson masses below about 140 GeV, i.e., in the $S\sim20$–25 event number range where detection of such a fluctuation over an intrinsic background rate of similar size should be relatively straightforward.

Of course, both the inclusive $\gamma\gamma$ and the associated $l\gamma\gamma X$ detection modes would benefit from better $M_{\gamma\gamma}$

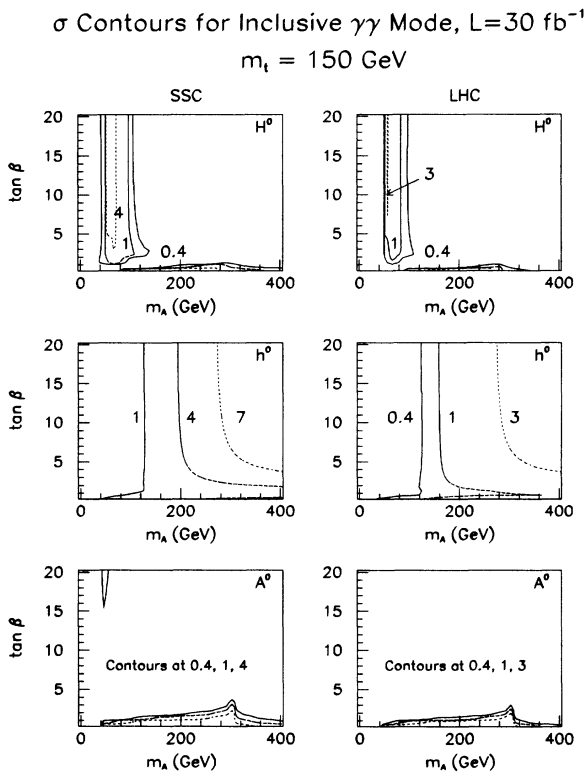

FIG. 15. Contours of $\sigma=S/\sqrt{B}$ for H^0, h^0, and A^0 detection in the inclusive $\gamma\gamma$ mode. We take $m_t=150$ GeV and $L=30$ fb^{-1}. Results are presented for both the SSC and LHC. Only the $\gamma\gamma$ continuum is included in B. The only cut employed for S and B is $|\cos\theta^*|<0.5$. No additional detector or jet-photon discrimination efficiencies are incorporated.

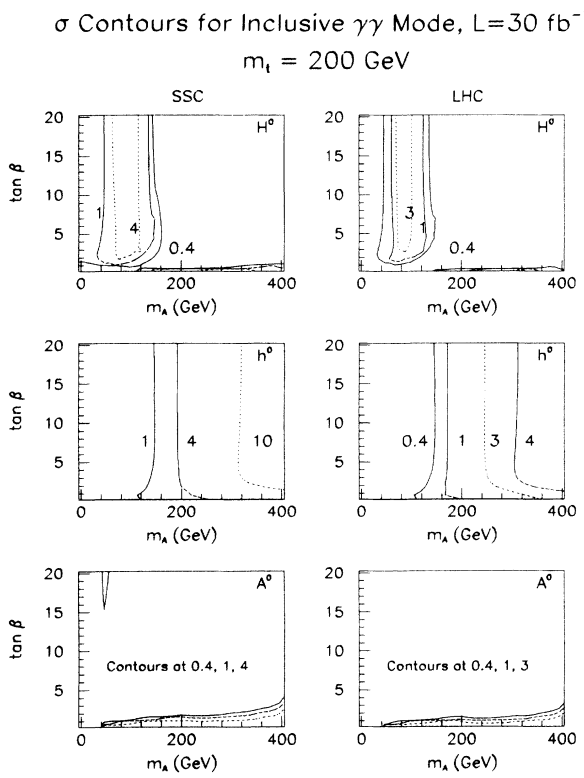

FIG. 16. Same as for Fig. 15, but for $m_t = 200$ GeV.

resolution than that quoted in Eq. (2) and typical of the SDC detector. As the $M_{\gamma\gamma}$ resolution improves, the inclusive $\gamma\gamma$ mode slowly becomes more competitive. But, after appropriate rescaling, our computations indicate that even for a 2% resolution (probably the best that could be achieved in a special purpose detector of reasonable cost) the $l\gamma\gamma$ mode provides more observable signals for the MSSM Higgs bosons than does the inclusive $\gamma\gamma$ mode. In practice, this may mean that a signal is first detected in the $l\gamma\gamma X$ mode, and later confirmed by a fluctuation in the $\gamma\gamma$ inclusive rate in the same mass bin.

V. OVERALL SURVEY AND $t \to H^+ b$ DETECTION

We will now turn to a detailed comparison of the utility of the $l\gamma\gamma$ detection mode for the neutral Higgs bosons to what can be achieved at LEP II, as represented by the 25-event contours of Fig. 2, and to other detection modes for the various MSSM Higgs bosons at the SSC.

A. Comparison of $l\gamma\gamma$, $4l$, and LEP II

We shall first give a $l\gamma\gamma, 4l$, LEP II comparison for the cases of $m_t = 100$, 150, and 200 GeV in turn.

For $m_t \sim 100$ GeV (not shown in Fig. 2), LEP II (with $\sqrt{s} = 200$ GeV and $L = 500$ pb^{-1}) will be able to discover the h^0 over essentially all of the $m_{A^0} \leq 400$ GeV and $0.5 \leq \tan\beta \leq 20$ region of parameter space considered here. There is only a very narrow region centered about $m_{A^0} \sim 65$ with $\tan\beta \gtrsim 6$ where neither the $h^0 Z$ nor the $h^0 A^0$ reaction satisfies the strict discovery criterion of 25 events for a 25% detection efficiency. If 15 events were adequate, then the h^0 could be detected in one reaction or the other at LEP II throughout all of parameter space. The SSC will be able to see the h^0 in the $l\gamma\gamma X$ mode for $m_{A^0} \gtrsim 250$ GeV and $\tan\beta \gtrsim 2$ (and thereby measure the $h^0\gamma\gamma$ coupling, which is of great interest as a probe of new heavy fermion loops), but will not be able to see the h^0 in the $4l$ mode (see Ref. [21]). Detection of the H^0 and A^0 in either the $l\gamma\gamma X$ mode or the $4l$ mode will be confined to very small regions of parameter space as indicated here and in Refs. [21,23].

For $m_t \sim 150$ GeV, the parameter region over which LEP II cannot detect $h^0 Z$ or $h^0 A^0$ production becomes significant (see Fig. 2). Much of the $m_{A^0} \gtrsim 60$ GeV and $\tan\beta \gtrsim 7$ region of parameter space will become inaccessible. However, for $m_t \sim 150$ GeV, Fig. 12 shows that h^0 detection in the $l\gamma\gamma X$ mode becomes possible at the SSC for $m_{A^0} \gtrsim 200$ GeV. This is fortunate since (as shown in Ref. [21]) h^0 detection in the $4l$ mode is not possible for this low a top mass. Meanwhile, H^0 detection in the $4l$ mode is possible when $m_t \sim 150$ GeV in the small region roughly characterized by 50 GeV $\lesssim m_{A^0} \lesssim 2m_t$, $\tan\beta \lesssim 3$ [21], and H^0 detection in the $l\gamma\gamma X$ mode is possible in the tiny region $m_{A^0} \sim 150$ GeV, $\tan\beta \geq 5$.

For $m_t \sim 200$ GeV, the portion of parameter space for which $h^0 Z$ or $h^0 A^0$ production at LEP II will be detectable becomes quite restricted. As shown in Fig. 2, $h^0 Z$ can be observed only if $\tan\beta$ and m_{A^0} are in the low $\tan\beta$, small m_{A^0} corner of parameter space. And the $h^0 A^0$ process provides a viable signal only if $m_{A^0} \lesssim 50$ GeV and $\tan\beta \gtrsim 2$. Fortunately, for this large a top-quark mass, the SSC will allow discovery of one or more of the neutral Higgs bosons throughout virtually the entire parameter space. From Fig. 13 we see that the h^0 is detectable in the $l\gamma\gamma X$ mode for $m_{A^0} \gtrsim 200$ GeV (and for even lower m_{A^0} values if $\tan\beta$ is small). Further, the H^0 becomes detectable via this mode in a significant wedge of parameter space where m_{A^0} lies between about 60 and 100 GeV and $\tan\beta \gtrsim 3$. In addition, as shown in Ref. [21], the $4l$ mode allows detection of either the h^0 or the H^0 throughout nearly *all* of parameter space. The h^0 can be detected in the $4l$ mode for $m_{A^0} \gtrsim 160$ GeV for $\tan\beta \gtrsim 2$; and the $4l$ decay of the H^0 produces a viable signal in the remarkably complementary region where $m_{A^0} \lesssim 160$ GeV at large $\tan\beta$, expanding to all m_{A^0} when $\tan\beta \lesssim 2.5$. In this domain, however, there is one small region, with $m_{A^0} \lesssim 17$ GeV and $\tan\beta \gtrsim 7.5$, where $H^0 \to 4l$ cannot be detected. Since neither the H^0 nor the h^0 can be detected in the $l\gamma\gamma X$ mode in this particular region, it is fortunate that the $h^0 A^0$ process would already have been detected at LEP and would certainly also be visible at LEP II for such parameter choices.

In the above discussion we have not considered detection of the A^0. In Figs. 11–13, we have seen that A^0 detection in the $l\gamma\gamma X$ mode is only possible in a very restricted region of parameter space. Not only must m_{A^0} be below $2m_t$, but also $\tan\beta$ must be $\lesssim 1$ in order that the

$A^0 \to b\bar{b}$ decay width not be very large, and thereby suppress the $A^0 \to \gamma\gamma$ branching ratio. As found in Ref. [23], precisely these same remarks apply to the $A^0 \to 4l$ mode.

B. A brief survey of other modes for h^0, H^0, and A^0 detection

Of course, other decay modes for the neutral MSSM Higgs bosons are worth examining at the SSC. First, we note that direct inclusive production followed by detection of any of the neutral Higgs bosons in $b\bar{b}$ decay modes is almost certainly impossible because of the large $b\bar{b}$ continuum backgrounds. Other possible detection modes include the following. If $m_{A^0} > m_Z + m_{h^0}$, one can consider detection in the $A^0 \to Zh^0 \to l^+l^-b\bar{b}$ mode [1,2,20,30]. But this mode is limited to parameter choices such that $\tan\beta$ is not too large (i.e., such that the $b\bar{b}$ width of the A^0 is not too enhanced). Although the $\tau^+\tau^-$ decay mode for the neutral Higgs bosons has a significant branching ratio at large $\tan\beta$, in inclusive production only approximate reconstruction of the Higgs-boson mass is possible (using a high-p_T jet tag) and backgrounds could be a problem [20]. Associated W+Higgs boson production, followed by $W \to l\nu$ and Higgs boson $\to \tau^+\tau^-$ is also under study, and may well provide a viable signal at large $\tan\beta$. Once the $t\bar{t}$ decay mode is kinematically allowed for the A^0 and H^0, detection in the production/decay channel $gg \to t\bar{t}A^0$ or $H^0 \to t\bar{t}t\bar{t}$ might be possible if efficient techniques for isolating the $4t$ final state can be found [31]. However, the $t\bar{t}$ branching ratio for the A^0 and H^0 is only significant if $\tan\beta$ is not large.

C. Detection of $t \to H^+b$ decays in $t\bar{t}$ events

As an important complement to detection of the neutral Higgs bosons of the MSSM, we now make a rough determination of the region of parameter space for which detection of the charged Higgs boson should be possible at the SSC and LHC. We shall see that this region can be quite substantial when m_t is large. Our starting point is to note that detailed studies [32] have shown that the high rate of $t\bar{t}$ production at the SSC allows detection of $t \to H^+b$ decays unless $B(t \to H^+b)$ is quite small. Typically, a very significant effect in either the $H^+ \to jj$ (dominant for small $\tan\beta$) or the $H^+ \to \tau^+\nu$ (dominant for $\tan\beta \gtrsim 1$) decay mode can be observed at the SSC for $L = 30$ fb^{-1} so long as $B(t \to H^+b) \gtrsim 0.01$.

In Fig. 17 we display contours of $B(t \to H^+b)$ for $m_t = 150$ and 200 GeV. Adopting the $B \geq 0.01$ criterion, one finds that, at the SSC, $H^\pm$ detection in top quark decays would be possible for $m_{A^0} \lesssim 100$ GeV (150 GeV) for $m_t = 150$ GeV (200 GeV), except for $\tan\beta$ values in the vicinity of 5 where the maximum m_{A^0} that can be probed in this way declines to ~ 90 GeV (~ 130 GeV). Of course, when $\tan\beta$ is $\lesssim 1$ and $m_{H^+} \sim m_W$ (corresponding to small m_{A^0}), H^+ detection will require a larger $t \to H^+b$ branching ratio than 0.01. This is because, for $\tan\beta \lesssim 1$, the H^+ decays primarily to jets and the jet-jet mass peak of the H^+ would become difficult to disentangle from the W^+ mass peak arising from $t \to W^+b$ decays. Fortunately, Fig. 17 shows that in this region of parameter space $B(t \to H^+b)$ is generally quite large. However, this detection mode for the H^+ does begin to fail below about $\tan\beta = 0.2$ for quite a different reason: to trigger upon the $t\bar{t}$ events we require that one of the t's decays to a leptonically ($l = e, \mu$) decaying W. As $\tan\beta$ falls below 0.2, $B(t \to H^+b) \to 1$ and there are too few W's emerging from the t decays for viable triggering.

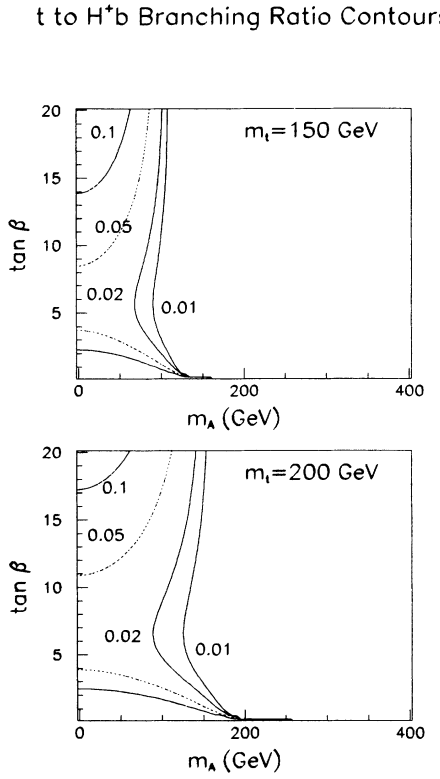

FIG. 17. Contours of $B(t \to H^+b)$ in m_{A^0}-$\tan\beta$ parameter space for $m_t = 150$ and 200 GeV. B values for the various contours appear on the plots.

This detection mode for the H^+ can also, of course, be employed at the LHC. At the LHC the rate for $t\bar{t}$ production is about a factor of 6 lower than at the SSC. Keeping in mind the fact that the background to $t \to H^+b$ detection also comes from $t\bar{t}$ production,[3] we see that for $L = 30$ fb^{-1} a viable signal will require $B(t \to H^+b) \gtrsim 0.025$. Figure 17 shows that this holds over a somewhat reduced region of parameter space. For $B(t \to H^+b) \sim 0.01$ to provide an adequate signal at the LHC will require integrated luminosity of order $L \sim 180$ fb^{-1}.

VI. FINAL CONCLUSIONS: TOWARDS A NO-LOSE THEOREM

Before concluding, it is important to reemphasize that all our results have assumed that chargino, neutralino,

[3]This implies that statistical significances will scale by the square root of this factor.

and squark pair states are not kinematically allowed as Higgs-boson decay channels in the range of parameter space considered. For the H^0, A^0, and H^+, which have masses up to of order 400 GeV in our parameter scan, this means that the lightest neutralino must be more massive than $\sim$200 GeV. Thus the supersymmetric parameters μ and M, which set the scale of chargino and neutralino masses, must be $\geq$400–500 GeV (the lightest chargino and neutralino typically have masses of order M and $\sim M/2$, respectively) in order for all the results we have obtained to apply. (In the simplest no-intermediate-scale grand unification scenario, this implies a gluino mass in excess of about 1.6 TeV.) For such chargino masses, and for squark masses $\gtrsim$ 1 TeV, we have checked that the chargino and squark loop contributions to the $\gamma\gamma$ couplings of the MSSM Higgs bosons have only a very small effect (usually $\lesssim$2%, but never more than 20%—the effects are only this large in regions where detection is not possible anyway). Should supersymmetric particle pair channels be kinematically allowed in the decay of the Higgs bosons, the associated widths are typically quite large [1]. Indeed, these channels can easily dominate the decays, and certainly the utility of the $\gamma\gamma$, $4l$, and $t\to H^+b$ detection modes that we have surveyed above would have to be reexamined. Most probably, it would be more advantageous to search for those MSSM Higgs bosons that decay into pairs of supersymmetric particles directly in the supersymmetric channels.

However, even if the threshold for supersymmetric-particle-pair decays is as low as 200 GeV, we can still draw an important overall conclusion: either h^0Z (and/or possibly h^0A^0) production will be seen at LEP II or one or more of the MSSM Higgs bosons will be detectable at the SSC, using the three relatively robust modes, specified above and surveyed in Sec. V, throughout all or almost all of parameter space for any value of m_t. To reiterate, the three SSC modes in question are as follows: detection of the h^0 or H^0 in the $4l$ decay mode, detection of the h^0 or H^0 using the $l\gamma\gamma X$ final state, and detection of $t\to H^+b$ decays in $t\bar{t}$ production events. The reason that the critical threshold limitation is at $\sim$200 GeV can be seen by examining the complementarity of the various modes in question as revealed in Figs. 8, 9, and 17, and the $4l$ contour figures of Ref. [21]. The crucial feature to note is that for moderate to large m_t, $H^0\to 4l$, $WH^0X\to l\gamma\gamma X$, and $t\to H^+b$ detection is only critical for $m_{A^0}\sim m_{H^0}\sim m_{H^+}\lesssim$200 GeV. For higher values of m_{A^0}, the $h^0\to 4l$ and/or $Wh^0X\to l\gamma\gamma X$ detection modes provide a viable signal since the h^0 is never as heavy as 200 GeV and thus would not decay to supersymmetric channels under the stated assumption. Thus the overall region in which at least one of the MSSM Higgs bosons can be detected in the robust SSC modes is not altered unless the supersymmetric particle pair states have a threshold below about 200 GeV.

It is also clear that LEP II and the SSC prove to be highly complementary. For a large top-quark mass, h^0Z and h^0A^0 detection at LEP II is confined to quite a small region of parameter space, whereas detection of the h^0 or H^0 is possible at the SSC throughout most of parameter space (in particular in the large portion of parameter space that cannot be covered at LEP II). As m_t decreases, the portion of parameter space that can be probed by the $4l$ and $l\gamma\gamma X$ modes at the SSC shrinks, while that which can be probed by LEP II expands. At $m_t=150$ GeV, the combined parameter space coverage of LEP II and the $4l, l\gamma\gamma X$ modes is no longer complete. There is a window of m_{A^0} between $\sim$65 and $\sim$185 GeV at larger tanβ where none of the neutral Higgs bosons can be detected in these modes. Detection of $t\to H^+b$ is possible, however, for m_{A^0} up to about 100 GeV for $m_t=150$ GeV. This leaves a window from $m_{A^0}\sim$100–185 GeV with tan$\beta\gtrsim 8$ for which other detection modes must be found. By $m_t=100$ GeV, h^0 detection at LEP II will be possible for virtually all of parameter space. Whereas, h^0 detection will only be possible at the SSC in the $l\gamma\gamma X$ mode and only if m_{A^0} is large and tan$\beta\gtrsim 2$.

We have attempted to summarize the above remarks in two figures. In Figs. 18 and 19 (for $m_t=150$ and 200

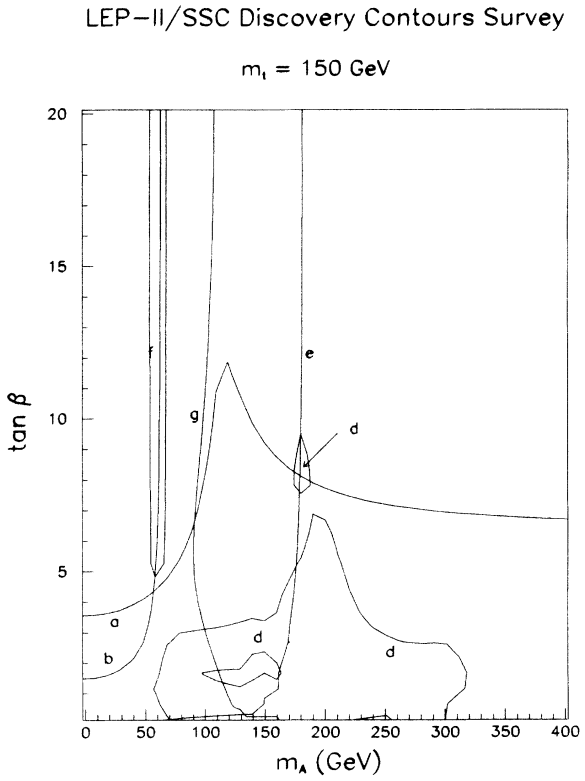

FIG. 18. Discovery contours in m_{A^0}-tanβ parameter space for the SSC with $L=30$ fb^{-1} and LEP II with $L=500$ pb^{-1} for the reactions: (a) $e^+e^-\to h^0Z$ at LEP II; (b) $e^+e^-\to h^0A^0$ at LEP II; (c) $h^0\to 4l$; (d) $H^0\to 4l$; (e) $Wh^0X\to l\gamma\gamma X$; (f) $WH^0X\to l\gamma\gamma X$; (g) $t\to H^+b$. We take $m_t=150$ GeV. Discovery criteria are as stated in the text: 25 events for reactions (a) or (b) at LEP II; $\sigma=4$ for reactions (c)–(f); and $B(t\to H^+b)\geq 0.01$ for (g). The contour corresponding to a given reaction is labeled by the letter assigned to the reaction above. In each case, the letter appears on the side of the contour for which detection of the particular reaction *is* possible.

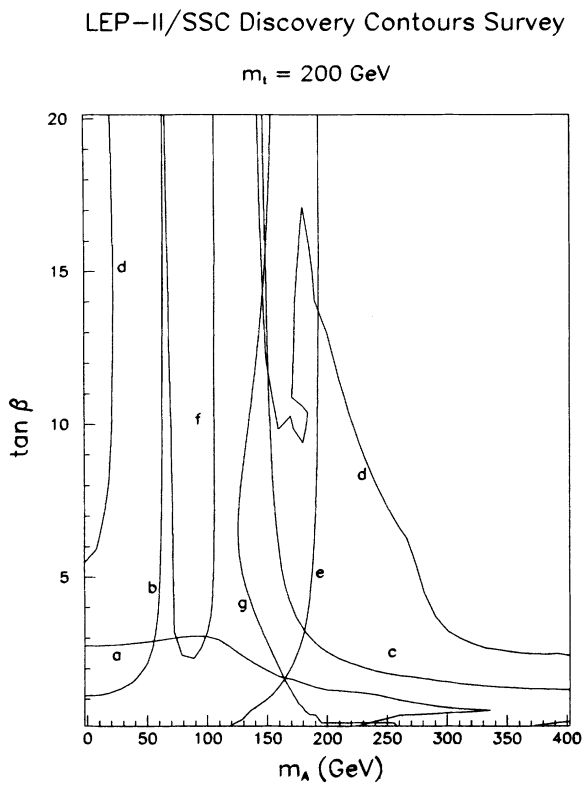

FIG. 19. Discovery contours for the SSC and LEP II as in Fig. 18, but for $m_t = 200$ GeV.

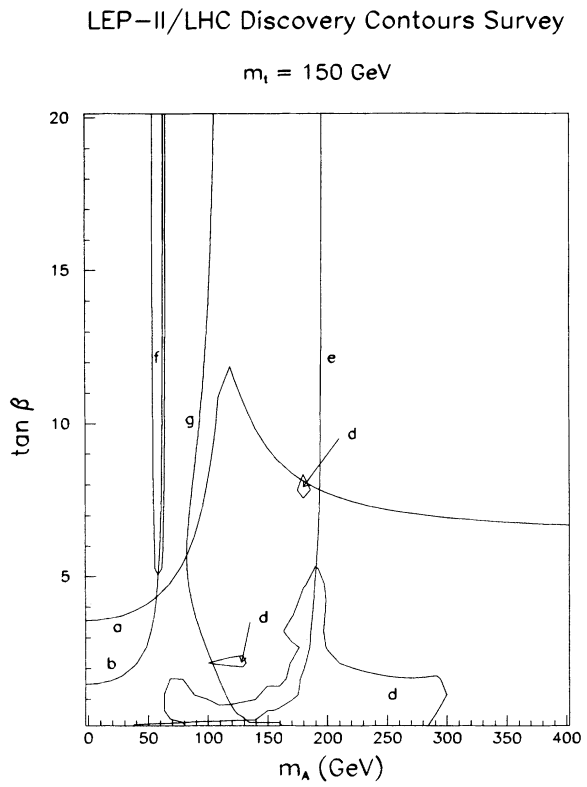

FIG. 20. LHC discovery contours at the enhanced luminosity of $L = 100$ fb^{-1} for $m_t = 150$ GeV. Also shown are LEP II $m_t = 150$ GeV discovery contours for $L = 500$ pb^{-1}. Labeling is the same as in Fig. 18. Discovery criteria are also as in Fig. 18, except that the discovery requirement for $t \to H^+ b$ decays at the LHC with $L = 100$ fb^{-1}, analogous to that employed for the SSC at $L = 30$ fb^{-1}, is $B(t \to H^+ b) \geq 0.0135$.

GeV, respectively) we present the m_{A^0}-tanβ parameter space SSC discovery contours for the robust reactions for which results were outlined above. In particular, these figures include $4l$ channel contours. Also shown are the LEP II discovery contours for $L = 500$ pb^{-1}. The discovery criteria we adopt for these figures are those discussed earlier: $\sigma = 4$ for the $l\gamma\gamma$ and $4l$ modes, $B(t \to H^+ b) \geq 0.01$ for $t \to H^+ b$ decays, and 25 events (for 25% detection efficiencies) for the $h^0 Z$ and $h^0 A^0$ modes at LEP II. (We assume $L = 30$ fb^{-1} for the SSC, and $L = 500$ pb^{-1} for LEP II.) By examining these figures closely, following the convention that contour labels always appear on the inside of the region where discovery in a particular reaction *is* possible, all the features described earlier will become apparent. In particular, in the $m_t = 150$ GeV case (Fig. 18), the small region of parameter space with $100 \lesssim m_{A^0} \lesssim 185$ GeV and tan$\beta \gtrsim 7$–12 that is not accessible via these reactions is easily isolated. And, for $m_t = 200$ GeV it should be obvious from Fig. 19 that there is substantial overlap of the various discovery regions, so that detection of one or more of the MSSM Higgs bosons will be possible at either LEP II or at the SSC throughout all of parameter space.

Results for the LHC can also be summarized in this same way. We have chosen to present results in the case of the LHC for the enhanced luminosity of $L = 100$ fb^{-1}.[4] The 100 fb^{-1} LHC discovery contours appear in Figs. 20 and 21, for $m_t = 150$ and 200 GeV, respectively. Certainly, one observes that there is a great deal of similarity between the 100 fb^{-1} LHC discovery regions and the 30 fb^{-1} SSC discovery regions. However, even at 100 fb^{-1} and for $m_t = 200$ GeV, the LHC cannot quite guarantee that one of the MSSM Higgs bosons will be discovered throughout all of parameter space in the robust modes analyzed here. Indeed, Fig. 21 displays a small region centered on $m_{A^0} \sim 160$ GeV, with tan$\beta \gtrsim 6$, where none of the discovery channels considered here would be viable. And, of course, for $m_t = 150$ GeV, Fig. 20 exhibits a substantial region, roughly $90 \lesssim m_{A^0} \lesssim 200$

[4]The appropriate contours from our earlier plots and those for the $4l$ mode from Ref. [21] can be obtained by rescaling: $\sigma = 4$ at $L = 100$ fb^{-1} corresponds to $\sigma = 2.2$ at $L = 30$ fb^{-1}. Further, after adjusting for the factor of ~ 6 decrease in the $t\bar{t}$ production cross section in going from the SSC to the LHC, one finds that the LHC $t \to H^+ b$ signal with $B(t \to H^+ b) = 0.0135$ is as detectable at $L = 100$ fb^{-1} as the corresponding SSC signal is for $B(t \to H^+ b) = 0.01$ at $L = 30$ fb^{-1}.

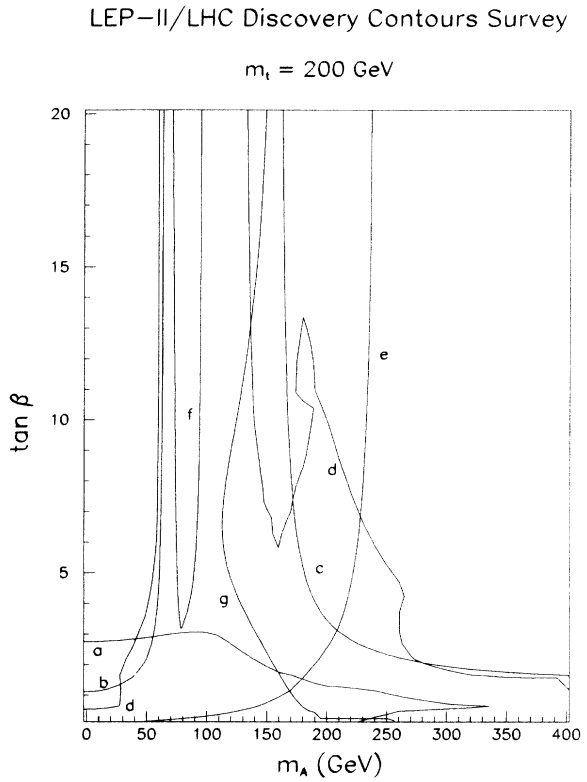

FIG. 21. Discovery contours for the LHC and LEP II as in Fig. 20, but for $m_t = 200$ GeV.

GeV with $\tan\beta \gtrsim 6-12$, that would be accessible neither at LEP II nor in the $h^0, H^0 \to 4l$; $Wh^0X, WH^0X \to l\gamma\gamma X$; or $t \to H^+ b$ channels at the LHC. Not surprisingly, if only $L = 10$ fb^{-1} is available at the SSC, the regions of inaccessible parameter space would be very similar to those exhibited in Figs. 20 and 21 for the LHC with $L = 30$ fb^{-1}.

Let us restate our most important overall conclusion, based on the above analysis and obtained under the assumptions that $L = 30$ fb^{-1} can be accumulated at the SSC and that the supersymmetric particle pair channels have thresholds beyond ~ 200 GeV. We have seen that LEP II and the SSC tend to be quite complementary; the decrease in LEP II coverage of MSSM parameter space as m_t increases tends to be compensated by the increasing coverage of the SSC. Despite the fact that the MSSM Higgs bosons are in general more difficult to detect than the SM ϕ^0 (and so some of the other modes outlines earlier for detecting them should not be overlooked), we have shown that if they exist, the MSSM Higgs bosons will be observable at LEP II or the SSC except for a gap in parameter space from $m_{A^0} \sim 100$ to 185 GeV with $\tan\beta \gtrsim 8$ for m_t around 150 GeV. Thus the h^0Z/h^0A^0 modes at LEP II, the very clean $4l$ and $l\gamma\gamma X$ modes at the SSC, and the high rate of $t\bar{t}$ production followed by $t \to H^+ b$ decay (when kinematically allowed) at the SSC, in combination, come close to providing an important no-lose theorem for the MSSM Higgs sector.

ACKNOWLEDGMENTS

This project originated at the U.C. Davis Workshop on Higgs/EWSB Physics at Hadron Super Colliders. One of us (J.F.G.) is also indebted to the Aspen Center for Physics where part of this work was completed. We are indebted to A. Ballestrero, E. Maina, and M. Mangano for providing us with extensions of their background computations. We also thank D. Dicus and R. Vega for conveying their preliminary results for the $t\bar{t}\gamma\gamma$ background to us. Discussions and collaboration with H. Haber are gratefully acknowledged by J.F.G. This work was supported in part by the Department of Energy and by the Texas National Research Laboratory Commission.

[1] J. F. Gunion, H. E. Haber, G. Kane, and S. Dawson, *The Higgs Hunter's Guide* (Addison-Wesley, Reading, MA, 1990).
[2] J. F. Gunion *et al.*, in *Research Directions for the Decade,* Proceedings of the Summer Study on High Energy Physics, Snowmass, Colorado, 1990, edited by E. L. Berger and I. Butler (World Scientific, Singapore, 1991).
[3] J. F. Gunion, in Proceedings of the Workshop on High Energy Physics Phenomenology-II, Calcutta, India, 1991 (unpublished).
[4] J. F. Gunion, G. L. Kane, and J. Wudka, Nucl. Phys. **B299**, 231 (1988).
[5] SDC Collaboration, Letter of Intent, No. SDC-90-00151 (unpublished).
[6] R. Kleiss, Z. Kunszt, and J. Stirling, Phys. Lett. B **253**, 269 (1991).
[7] M. Mangano, SDC Collaboration Note SSC-SDC-90-00113 (unpublished).
[8] J. F. Gunion, Phys. Lett. B **261**, 510 (1991).
[9] W. Marciano and F. Paige, Phys. Rev. Lett. **66**, 2433 (1991).
[10] Z. Kunszt, Z. Trocsanyi, and W. J. Stirling, Phys. Lett. B **271**, 247 (1991).
[11] A. Ballestrero and E. Maina, Phys. Lett. B **268**, 437 (1991).
[12] J. F. Gunion and L. Roszkowski, in *Research Directrons for the Decade* [2].
[13] V. Barger and K. Whisnant, Phys. Rev. D **43**, 1443 (1991).
[14] H. E. Haber and R. Hempfling, Phys. Rev. Lett. **66**, 1815 (1991).
[15] J. Ellis, G. Ridolfi, and F. Zwirner, Phys. Lett. B **257**, 83 (1991); **262**, 477 (1991); A. Brignole, J. Ellis, G. Ridolfi, and F. Zwirner, *ibid.* **271**, 123 (1991).
[16] Y. Okada, M. Yamagushi, and T. Yanagida, Prog. Theor. Phys. **85**, 1 (1991); Phys. Lett. B **262**, 54 (1991).
[17] R. Barbieri and M. Frigeni, Phys. Lett. B **258**, 395 (1991).
[18] A. Yamada, Phys. Lett. B **263**, 233 (1991).
[19] H. E. Haber and R. Hempfling (unpublished).
[20] Z. Kunszt and F. Zwirner, in *Proceedings of the ECFA Large Hadron Collider Workshop,* Aachen, Germany, 1990, edited by G. Jarlskog and D. Rein (CERN Report

No. 90-10, Geneva, Switzerland, 1990), Vol. II, p. 578.
[21] R. Bork, J. F. Gunion, H. E. Haber, and A. Seiden (unpublished).
[22] Z. Kunszt and F. Zwirner (unpublished).
[23] J. F. Gunion, H. E. Haber, and C. Kao (unpublished).
[24] As we were completing our paper, we received a closely related paper on the inclusive search mode: H. Baer, M. Bisset, C. Kao, and X. Tata, Phys. Rev. D **46**, 1067 (1992).
[25] P. N. Harriman, A. D. Martin, W. J. Stirling, and R. G. Roberts, Phys. Rev. D **42**, 798 (1990).
[26] SDC Collaboration, Technical Design Report No. SDC-92-201, 1992 (unpublished).
[27] D. Dicus and S. Willenbrock, Phys. Rev. D **39**, 751 (1989).
[28] H. Baer and J. F. Owens, Phys. Lett. B **205**, 377 (1988).
[29] D. Dicus and S. Willenbrock, Phys. Rev. D **37**, 1801 (1988).
[30] M. Felcini, J. F. Gunion, and C. P. Yuan (unpublished).
[31] J. F. Gunion and L. H. Orr (unpublished).
[32] R. M. Barnett, J. F. Gunion, H. E. Haber, I. Hinchliffe, B. Hubbard, and H.-J. Trost, SSC Report No. SDC-90-00141, 1990 (unpublished); R. M. Godbole and D. P. Roy, Phys. Rev. D **43**, 3640 (1991); L* Collaboration, Letter of Intent No. SSCL-SR-1154, 1990 (unpublished); EMPACT Collaboration, Letter of Intent No. SSCL-SR-1155, 1990 (unpublished).